Supporting Information for

$Ag_xH_{3-x}PMo_{12}O_{40}$/Ag nanorods/g-$C_3N_4$ 1D/2D Z-scheme heterojunction for high efficient visible-light photocatalysis

Xinyu Zhao[a], Yi Zhang[a], Yingnan Zhao[a], Huaqiao Tan[a,*], Zhao Zhao[a], Hongfei Shi[a,b]*, Enbo Wang[a], Yangguang Li[a,*]

[a] *Key Laboratory of Polyoxometalate Science of Ministry of Education, Faculty of Chemistry, Northeast Normal University, Changchun, 130024, P. R. China*

[b]*InstituteofPetrochemicalTechnology,JilinInstitutofChemicalTechnology,Jilin,132022, P. R.China*

Corresponding authors

Key Laboratory of Polyoxometalate Science of Ministry of Education, Faculty of Chemistry, Northeast Normal University, Changchun, 130024, P. R. China

E-mail address:tanhq870@nenu.edu.cn (H.Q. Tan); shihf813@nenu.edu.cn (H.F. Shi); liyg658@nenu.edu.cn (Y.G. Li);

Postal address: Northeast Normal University, Renmin Street No. 5268, Changchun, Jilin Province, 130024, P. R. China

2.1 Chemicals and Reagents.

Silver nitrate ($AgNO_3$) and Phosphomolybdic acid ($H_3PMo_{12}O_{40}$) were purchased from Sinopharm Chemical Reagent Co., Ltd, Urea ($CO(NH_2)_2$), Sodium sulfate (Na_2SO_4), Isopropanol (C_3H_7OH), 4-Hydroxy-TEMPO, Methyl orange (MO), Triethanolamine, Barium sulfate ($BaSO_4$), $K_2Cr_2O_7$ were purchased from Aladdin Chemical Co., Ltd., China. The purity of all reagents is analytical (AR) and not further purified.

2.2 Characterization Methods.

The surface morphology of the photocatalysts has been performed on a JEOL JSM 4800F SEM. Transmission electron microscopy (TEM) and HRTEM images were characterized utilizing a JEM-2100F microscope at an acceleration voltage of 200 kV. X-Ray diffraction measurements were carried out on a Bruker AXS D8 Focus by filtered Cu Ka radiation (λ= 1.54056 Å). X-ray photoelectron spectra were obtained applying an ESCALABMKII spectrometer with an Al-Kα achromatic X-ray source. The UV-Vis diffuse reflectance spectra (DRS) measurements were received by a UV-2600 UV-Vis spectrophotometer (Shimadzu), and $BaSO_4$ was employed as a background. The PL spectra were gained on a Hitachi F-7000 spectrophotometer with the excitation wavelength of 380 nm. Fourier Transform Infrared spectra (FTIR) were derived from Perkin Elmer Fourier Transform Infrared Spectrometer GX. The N_2 absorption–desorption isotherms were determined at 77 K with a Micromeritics Autosorb IQ instrument.

2.3 Photoelectrochemical Measurements.

Photocurrent measurements were carried out using a CHI700E Electrochemical Workstation in a common three-electrode configuration including a reference electrode, counter electrode and working electrode in a quartz cell. Ag/AgCl electrode and Pt foil were used as the reference electrode and counter electrode, respectively. A 300 W Xe lamp (CEL-HXF300, AULIGHT) was utilized as the light source, and a 0.5 M Na_2SO_4 solution was employed as the electrolyte. The working electrodes were prepared as the following method: 30 mg of different samples were dispersed in 1 mL of ethanol with sonication for 30 min to obtain slurry. Subsequently, the mixture was evenly dropped onto a 1×3 cm^2 FTO glass substrate. Finally, the prepared electrodes were air-dried at room temperature to gain the working electrodes.

2.4 Electrochemical Impedance Spectroscopy (EIS) Measurements.

The EIS measurement was tested using a CHI700E electrochemistry station in 0.5 M Na_2SO_4 with a frequency range from 0.01 Hz to 10 kHz at -0.2 V. The EIS data were recorded using a normal three-electrode system, in which samples on FTO glass with an active area of ca. 2.0 cm^2 were prepared as the working electrode, Pt wire as a counter electrode, and Ag/AgCl as a reference electrode.

2.5 Photocatalytic Tests.

The photocatalytic activities of the as-obtained specimens were evaluated by the photodegradation of MO and photoreduction of $K_2Cr_2O_7$. A glass vessel with a water-cooling jacket was applied as reactor, and a 300 W Xe lamp was employed as visible-light source with a 420 nm cut-off filter. Briefly, 20 mg of different samples were dispersed into a solution, which contains 20 mL of MO solution (20 $mg \cdot L^{-1}$; pH=1),

40 mL of $K_2Cr_2O_7$ solution (80 mg·L^{-1}; V_{H2O}:$V_{isopropanol}$ =1) or 20 mL tetracycline (20 mg·L^{-1}). Before the light irradiation, the mixture was stirred in darkness for a certain time interval until adsorption-desorption equilibrium. Subsequently, the light source was switched on, and further stirring was applied. Afterward, 1 mL of the reaction solution was extracted and centrifuged at constant time intervals. The supernatant of MO, $K_2Cr_2O_7$ and TC were detected using a Shimadzu UV-2600 UV-Vis spectrophotometer. The degradation efficiency was calculated by C/C_0, where C represents the concentration of trace MO, $K_2Cr_2O_7$ and TC solution at each irradiated time, and C_0 stands for the concentration before light irradiation.

2.6 Active Species Trapping Experiment.

We conducted the radical-trapping experiments aiming to explore the major active species in the photocatalytic degradation process of MO. In our study, the 4-Hydroxy-TEMPO, triethanolamine (TEOA), and isopropanol (IPA) were employed as superoxide radical ($\cdot O_2^-$) scavenger, hole (h^+) scavenger, and hydroxyl radical (·OH) scavenger, respectively. Typically, 20 mg of APM-4/C_3N_4-3 sample and different scavenger were dispersed in 20 mL of MO (20 ppm) aqueous solution and the following process was similar to the MO degradation test.

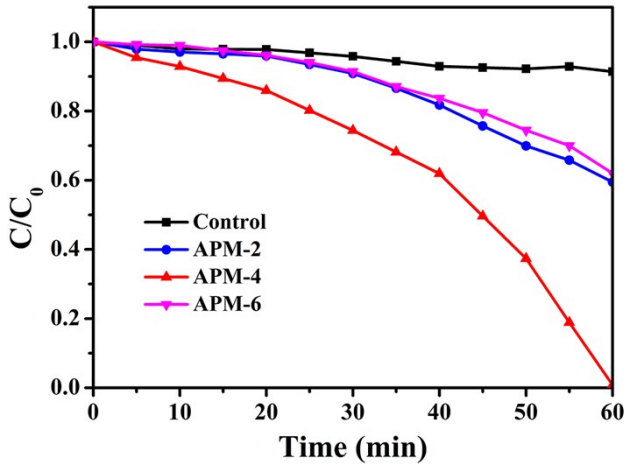

Figure S1. The profiles of photodegradation of MO by APM-2, APM-4, APM-6.

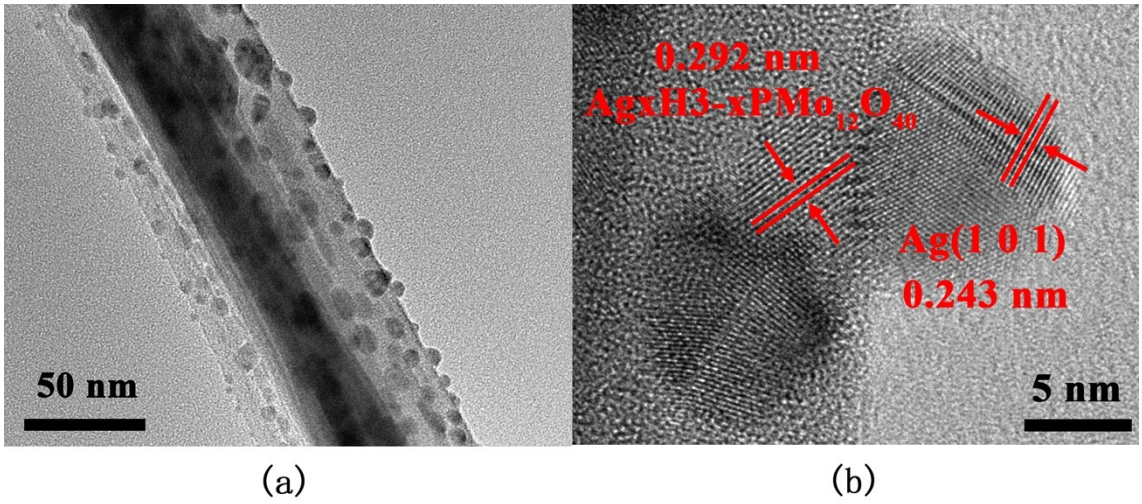

Figure S2. The TEM (a) and HRTEM (b) images of APM-4.

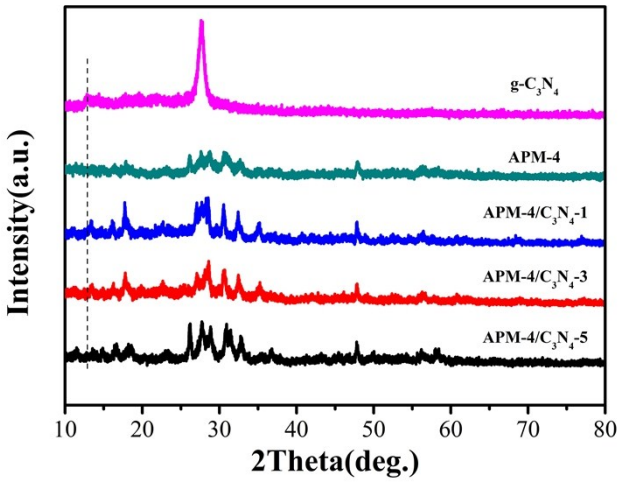

Figure S3. The XRD patterns of g-C_3N_4, APM-4, APM-4/C_3N_4-y (y=1, 3, 5 respectively).

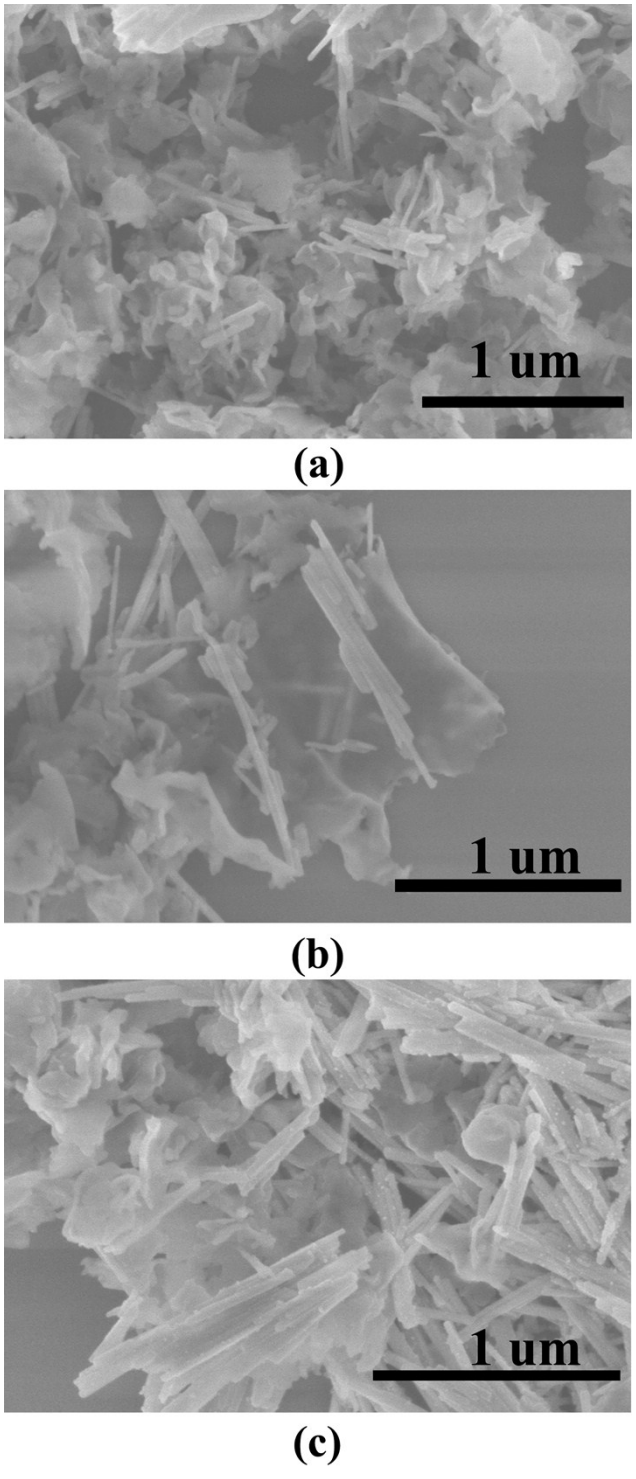

Figure S4. The SEM of APM-4/C_3N_4-1, APM-4/C_3N_4-3 and APM-4/C_3N_4-5.

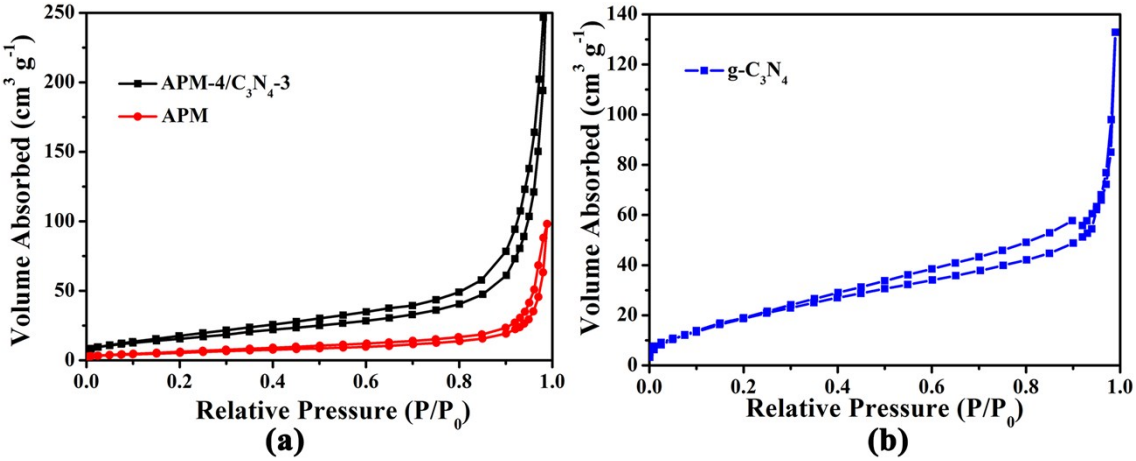

Figure S5. The N_2 adsorption-desorption isotherms of (a) APM-4 and APM-4/C_3N_4-3, (b) g-C_3N_4. The BET surface areas of APM-4, APM-4/C_3N_4-3 and g-C_3N_4 were 20.255, 57.236 and 77.220 $m^2 \cdot g^{-1}$, respectively.

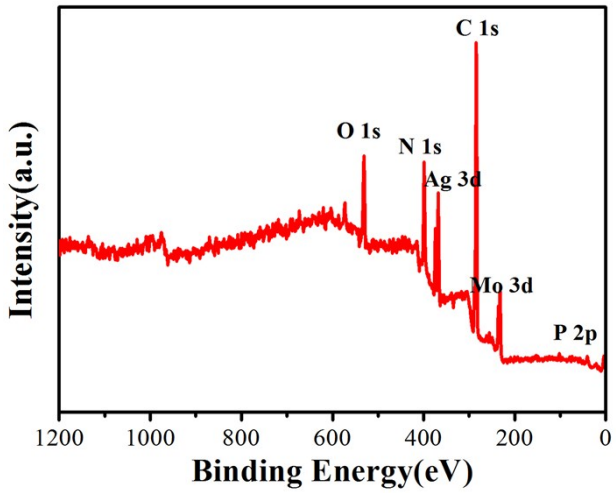

Figure S6. The full XPS spectra of APM-4/C_3N_4-3.

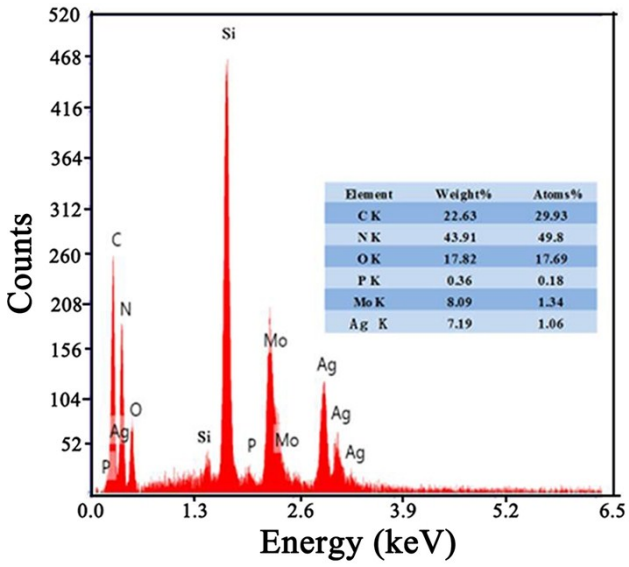

Figure S7. the EDX of APM-4/C_3N_4-3 sample.

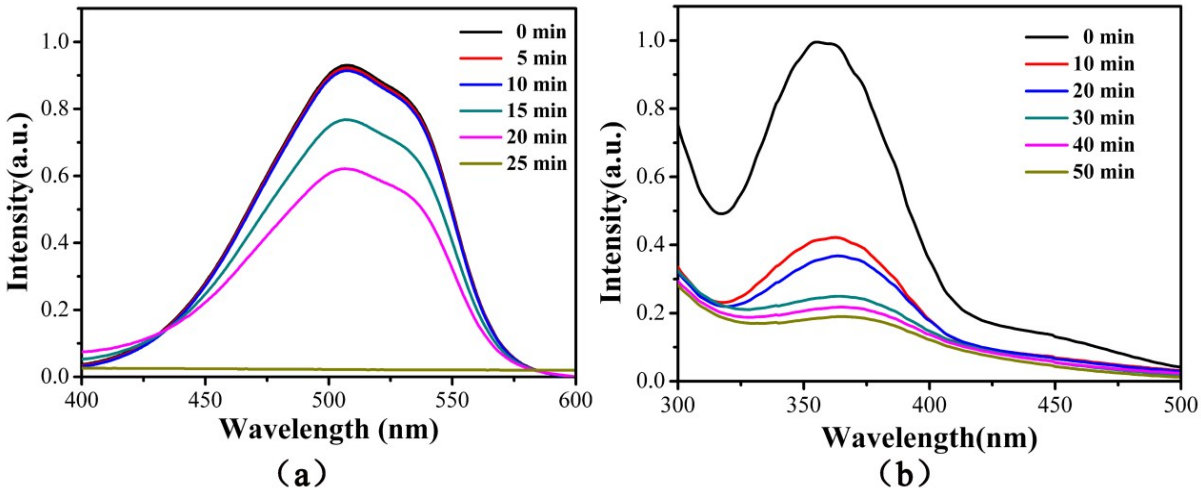

Figure S8. The curves of (a) photocatalytic degradation of MO and (b) photoreduction of Cr(VI) for APM-4/C_3N_4-3 under visible light irradiation (λ>420 nm).

Table S1. The photodegradation of MO under visible-light irradiation (λ> 420 nm) for APM-4/C_3N_4-3 in comparison with other catalysts[1-16].

Catalyst	$C_{Catalyst}$	C_{MO}	Time	Efficiency	λ_{light}	references
4-I/C-TiO_2	0.5 g L^{-1}	20 mg L^{-1}	25 min	94.2%	λ ≥ 400 nm	[1]
$(BiO)_2OHCl$	0.5 g L^{-1}	12.5 mg L^{-1}	90 min	80%	λ < 400 nm	[2]
ZHS–H–GR	0.25 g L^{-1}	10 mg L^{-1}	15 min	86.5%	λ = 254 nm	[3]
rGO/Cu_2O	1 g L^{-1}	20 mg L^{-1}	50 min	90%	visible-light	[4]
Sn-RGO	0.5 g L^{-1}	20 mg L^{-1}	4 min	Almost 100%	λ ≥ 420 nm	[5]
PC800	0.5 g L^{-1}	30 mg L^{-1}	6 h	69%	λ ≥ 420 nm	[6]
Cu_2O–O/TiO_2–QD	0.25 g L^{-1}	30 mg L^{-1}	60 min	97%	visible-light	[7]
CN/GOAs	/	20 mg L^{-1}	40 min	91.1%	λ ≥ 420 nm	[8]
BCS-30	1 g L^{-1}	10 mg L^{-1}	50 min	93.7%	λ ≥ 420 nm	[9]
Pt/$Bi1_2O_{17}Cl_2$	2 g L^{-1}	10 mg L^{-1}	3 h	97%	λ ≥ 400 nm	[10]
Ag/AgBr/g-C_3N_4@NGA	/	10 mg L^{-1}	30 min	96 %	λ ≥ 420 nm	[11]
m-Bi_2O_4/NCDs	0.5 g L^{-1}	10 mg L^{-1}	30 min	97.4 %	λ ≥ 420 nm	[12]
Cu_2O/Cu/AgBr/Ag	0.4 g L^{-1}	7 mg L^{-1}	50 min	98 %	λ ≥ 420 nm	[13]
Ag_2CrO_4/g-C_3N_4-N	0.4 g L^{-1}	10 mg L^{-1}	21 min	90 %	λ ≥ 400 nm	[14]
Ag_3PO_4/Ag/SiC	1 g L^{-1}	10 mg L^{-1}	15 min	97%	λ ≥ 420 nm	[15]
Ag_2CO_3/Ag/WO_3	0.5 g L^{-1}	10 mg L^{-1}	90 min	86.1%	λ ≥ 420 nm	[16]
Our work	1 g L^{-1}	20 mg L^{-1}	10 min	Almost 100%	λ ≥ 420 nm	/

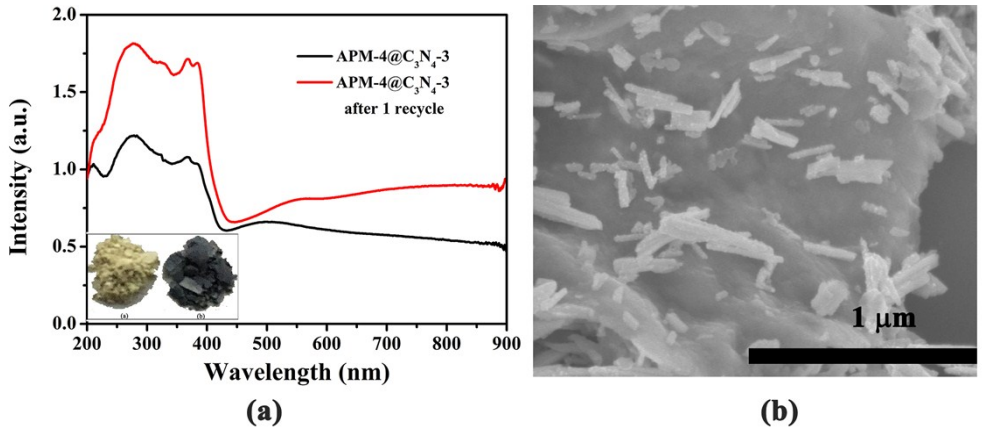

Figure S9. (a) The UV-vis diffuse reflectance spectra of APM-4/C_3N_4-3 sample (black line) and the recovered sample after one cycle experiment (red line).(b) The SEM of APM-4/C_3N_4-3 after recycle experiments. The illustration is optical images of (a) APM-4/C_3N_4-3 sample; (b) the recovered sample after one cycle experiment.

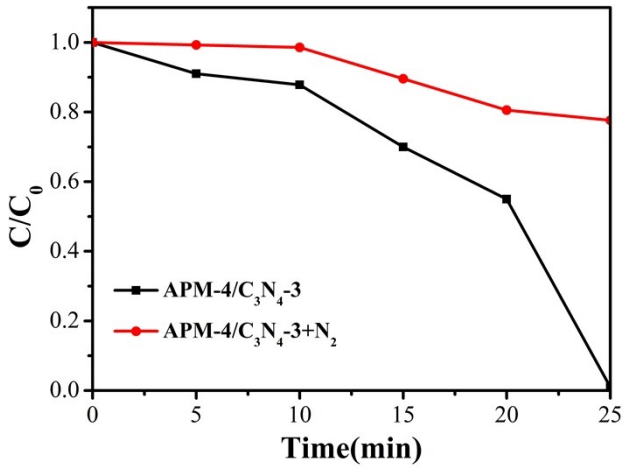

Figure S10. The effect of pouring N_2 into reaction system on the photodegradation activity of MO for APM-4/C_3N_4-3.

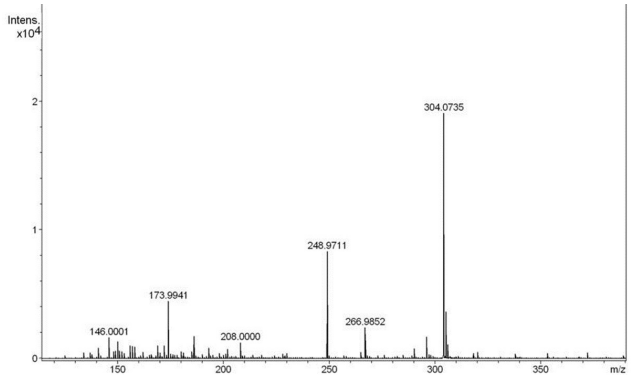

(a)

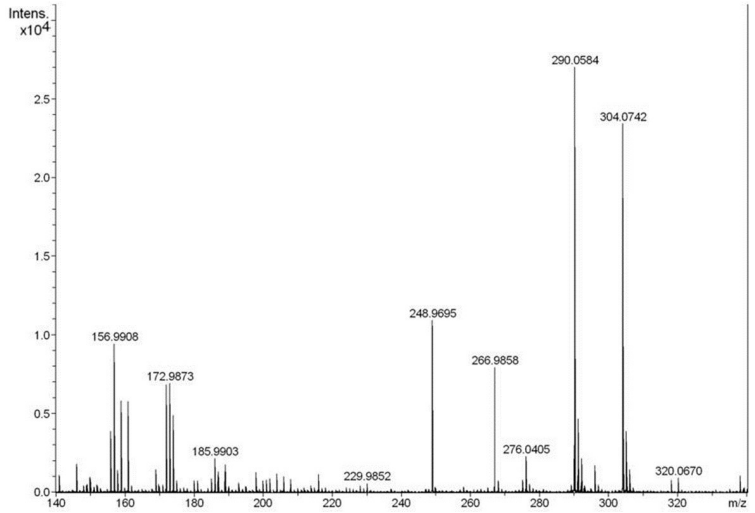

(b)

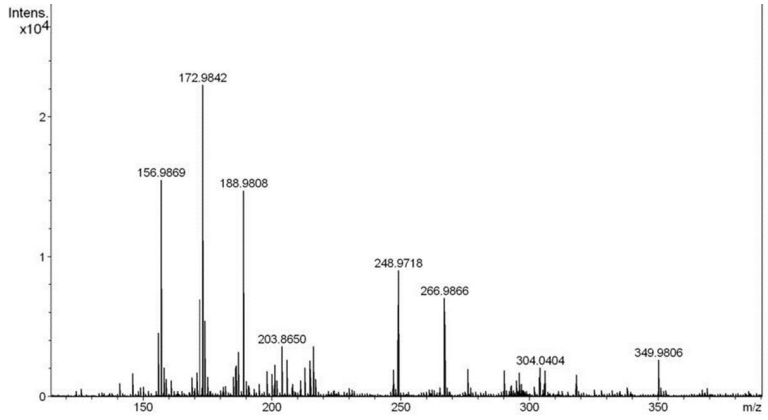

(c)

Figure S11. The main intermediate products generated during the process of photocatalytic degradation of MO for (a) 0, (b) 15 and (c) 30 min by APM-4/C_3N_4-3.

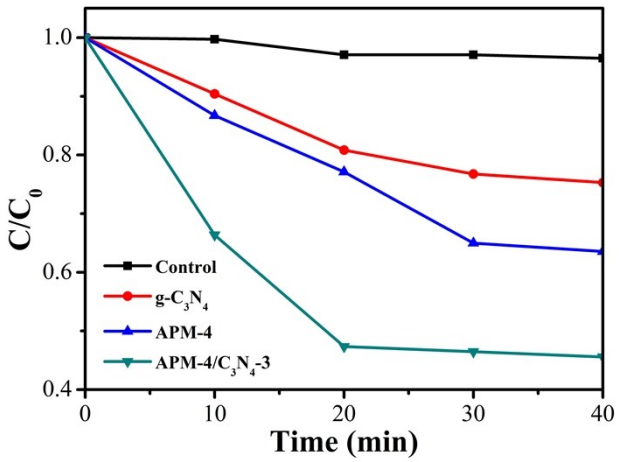

Figure S12. The profiles of photodegradation of tetracycline (TC) by g-C_3N_4, APM-4 and APM-4/C_3N_4-3 samples.

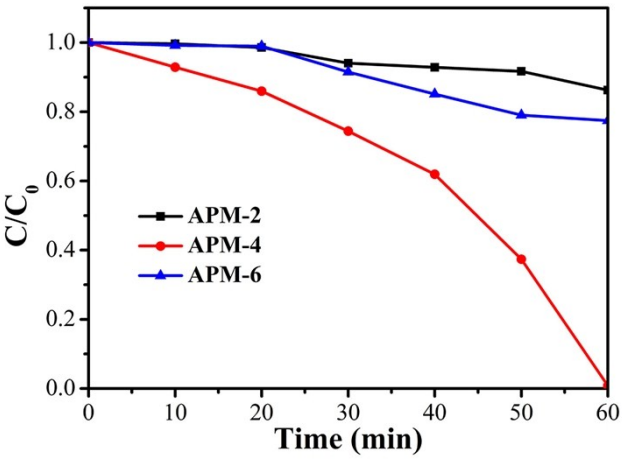

Figure S13. The profiles of photocatalytic reduction of Cr(VI) by APM-2, APM-4 and APM-6.

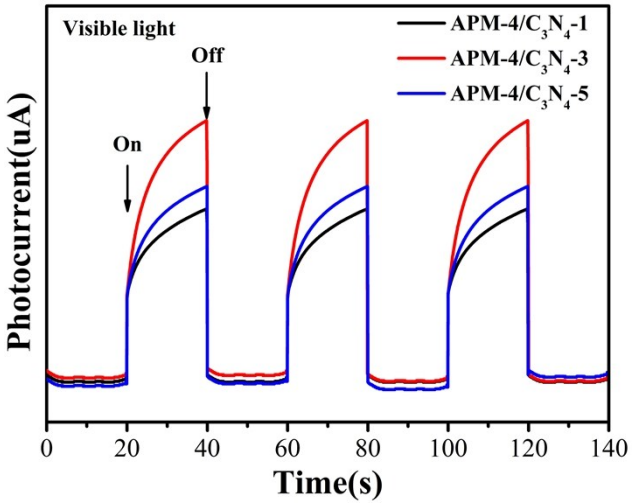

Figure S14. The transient photocurrent responses of APM-4/C_3N_4-y (y=1, 3, 5 respectively).

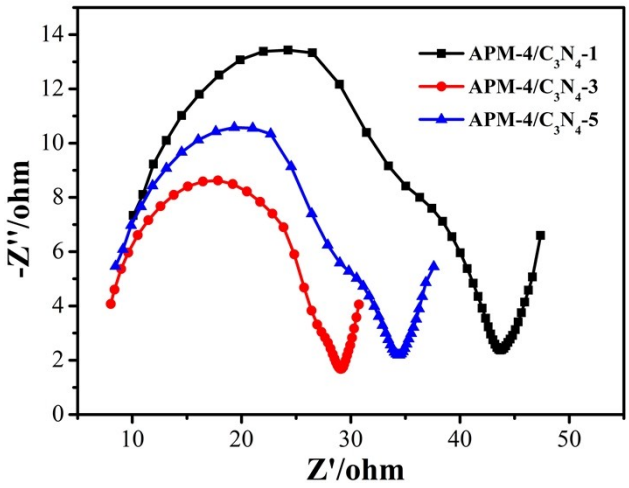

Figure S15. The EIS Nyquist plots for APM-4/C_3N_4-y (y=1, 3, 5 respectively).

References

[1] J. C. Wang, H. H. Lou, Z. H. Xu, C. X. Cui, Z. J. Li, K. Jiang, Y. P. Zhang, L. B. Qu, W. N. Shi, *J. Hazard. Mater.,* 2018, **360**, 356–363.

[2]Y. F. Zhai, A. Zhang, F. Teng, Y. Yang, W. H. Gu, W. Y. Hao, Z. L. Liu, Z. Liu, J. Y. Yang, Y. R. Teng, *Applied Catalysis B: Environmental,* 2018, **224**, 116–124.

[3] W. H. Feng, Z. X. Pei, Z. B. Fang, M. L. Huang, M. L. Lu, S. X. Weng, Z. Y. Zheng, J. Hu and P. Liu, *J. Mater. Chem. A.*, 2014, **2**, 7802–7811.

[4] X. Q. Liu, Z. Li, W. Zhao, C. X. Zhao, Y. Wang, Z. Q. Lin, *J. Mater. Chem. A*., 2015, **3**, 19148–19154.

[5] X. Y. Pan, Z. G. Yi, *ACS Appl. Mater. Interfaces.*, 2015, **7**, 27167-27175.

[6] M. M. Wan, X. D. Sun, Y. Y. Li, J. Zhou, Y. Wang, J. H. Zhu, *ACS Appl. Mater. Interfaces.*, 2016, **8**, 1252-1263.

[7] X. Xu, Z. H. Gao, Z. D. Cui, Y. Q. Liang, Z. Y. Li, S. L. Zhu, X. J. Yang, J. M. Ma, *ACS Appl. Mater. Interfaces.,* 2016, **8**, 91-101.

[8] L. Tang, C. T. Jia, Y. C. Xue, L. Li, A. Q. Wang, G. Xu, N. Liu, M. H. Wu, *Applied Catalysis B: Environmental*, 2017, **219**, 241–248.

[9] B. Wang, W. H. Feng, L. L. Zhang, Y. Zhang, X. Y. Huang, Z. B. Fang, P. Liu, *Applied Catalysis B: Environmental*, 2017, **206**, 510–519.

[10] C. J. Bi, J. Cao, H. Lina, Y. J. Wang, S. F. Chen, *Applied Catalysis B: Environmental,* 2016, **195**, 132–140.

[11] Y. X. Chen, P. L. Wang, Y. Liang, M. J. Zhao, Y. Y. Jiang, G. T. Wang, P. Zou, J. Zeng, Y. S. Zhang, Y. Wang, *Journal of Colloid and Interface Science,* 2019, **536**, 389–398.

[12] X. Y. Yue, X. L. Miao, Z. Y. Ji, X. P. Shen, H. Zhou, L. R. Kong, G. X. Zhu, X. Y. Li, S. A. Shah, *Journal of Colloid and Interface Science, 2018,* **531**, 473–482.

[13] J. He, D. W. Shao, L.C. Zheng, L. J. Zheng, D. Q. Feng, J. P. Xu, X. H. Zhang, W. C. Wang, W. H. Wang, F. Lu, H. Dong, Y. H. Cheng, H. Liu, R. K. Zheng,

Applied Catalysis B: Environmental, 2017, **203**, 917–926.

[14] Y. C. Deng, L. Tang, G. M. Zeng, J. J. Wang, Y. Y. Zhou, J. J. Wang, J. Tang, Y. N. Liu, B. Peng, F. Chen, *Journal of Molecular Catalysis A: Chemical,* 2016, **421**, 209–221.

[15] Z. H. Chen, F. Bing, Q. Liu, Z. G. Zhang, X. M. Fang, *J. Mater. Chem. A.,* 2015, **3**, 4652–4658.

[16] X. Z. Yuan, L. B. Jiang, X. H. Chen, L. J. Leng, H. Wang, Z. B. Wu, T. Xiong, J. Liang. G. M. Zeng, *Environ. Sci.: Nano*., 2017, **4**, 2175–2185.